SCIENCE CHINA
Information Sciences

• RESEARCH PAPER •

June 2021, Vol. 64 162401:1–162401:8
https://doi.org/10.1007/s11432-020-3035-8

Silicon-based inorganic-organic hybrid optoelectronic synaptic devices simulating cross-modal learning

Yayao LI[1], Yue WANG[1], Lei YIN[1], Wen HUANG[1], Wenbing PENG[1], Yiyue ZHU[1], Kun WANG[1], Deren YANG[1] & Xiaodong PI[1,2*]

[1]*State Key Laboratory of Silicon Materials, School of Materials Science and Engineering, Zhejiang University, Hangzhou* 310027*, China;*
[2]*Advanced Semiconductor Research Institute, ZJU-Hangzhou Global Scientific and Technological Innovation Center, Hangzhou* 311215*, China*

Received 14 March 2020/Revised 8 May 2020/Accepted 17 August 2020/Published online 16 March 2021

Abstract With advances in Si-based technology infrastructures and the rapid integration of Si-based optoelectronics, Si-based optoelectronic synaptic devices have the potential to greatly facilitate the large-scale deployment of neuromorphic computing. The incorporation of solution-processable polymer semiconductors into Si-based optoelectronics may enable the cost-effective fabrication of optoelectronic synaptic devices. Poly(3-hexylthiophene) (P3HT) is a semiconducting polymer used to manufacture optoelectronic synaptic transistors with P3HT channels and Si gates. The gate dielectric between them consists of a SiO_2 layer. Hybrid inorganic-organic Si/P3HT optoelectronic synaptic transistors can mimic synapses when exposed to optical and electrical stimuli. The Si/P3HT synaptic devices can spatiotemporally integrate optical and electrical stimuli to mimic cross-modal learning.

Keywords poly(3-hexylthiophene), silicon, optoelectronic synaptic devices, cross-modal learning, transistor

Citation Li Y Y, Wang Y, Yin L, et al. Silicon-based inorganic-organic hybrid optoelectronic synaptic devices simulating cross-modal learning. Sci China Inf Sci, 2021, 64(6): 162401, https://doi.org/10.1007/s11432-020-3035-8

1 Introduction

The performance of conventional neuromorphic computing based on complementary metal-oxide semiconductors (CMOSs) and silicon (Si) transistors is impressive [1, 2]. However, the enormous amount of energy consumed by conventional neuromorphic computing is becoming increasingly problematic [3, 4]. This has prompted the development of novel devices with ultra-low energy requirements that can simulate synapses in biological neural networks [5–10]. Synaptic devices can be used to build an artificial neural network (ANN) for neuromorphic computing. An ANN is an integrated system, so it would ideally be constructed using Si-based synaptic devices. This is because an advanced Si-based infrastructure can greatly facilitate large-scale integration, which is critical to the commercialization of neuromorphic computing.

It has become clear that the development of Si-based technologies largely hinges on optoelectronic integration [11,12]. Si-based optoelectronic integration should thus be improved for the realization of high-performance neuromorphic computing. The advantages of optoelectronic synaptic devices include wide bandwidths, excellent interconnectivity, negligible resistance-capacitance (RC) delays, and high power efficiency [13]. In order to make full use of these advantages, Si-based optoelectronic synaptic devices should be proactively investigated [14–18]. Research on traditional Si-based optoelectronic devices, such as solar cells [19], photodetectors [20], and light-emitting devices [21], indicates that Si-based hybrid structures are ideal for the fabrication of optoelectronic synaptic devices [15, 22–25]. The capabilities of Si and organic semiconductor hybrid structures are of particular interest for cost-effective processing

* Corresponding author (email: xdpi@zju.edu.cn)

at low temperatures [26]. However, few of the organic semiconductors including small molecules have been employed to construct hybrid structures with Si, and thermal evaporation in a vacuum could be specially required for the process [27–30]. Semiconducting polymers are amenable to solution processing, which could further simplify device fabrication [31]. Poly(3-hexylthiophene) (P3HT) is one of the most important semiconducting polymers, because its optical and electrical properties make it readily adaptable for use in traditional optoelectronic devices [32–35]. Hence, Si/P3HT hybrid structures are of interest for the fabrication of emerging optoelectronic synaptic devices.

In this study, we fabricated hybrid optoelectronic synaptic transistors that responded to both optical and electrical stimuli. We selected Si and P3HT to serve as the back gates and channels, respectively. The devices exhibited important synaptic features, such as excitatory postsynaptic current (EPSC), inhibitory postsynaptic current (IPSC), paired pulse facilitation (PPF), spike-number-dependent plasticity (SNDP), and spike-rate-dependent plasticity (SRDP). Significantly, the devices could be used to simulate cross-modal learning with a combination of optical and electrical stimuli.

2 Experimental section

2.1 Device fabrication

Si substrates with 200 nm thick, thermally grown SiO_2 layers were sequentially ultrasonicated in acetone, isopropyl alcohol, and absolute ethanol for 30 min. The substrates were dried under streaming nitrogen gas and subjected to ultraviolet (UV) ozone treatment for 15 min. They were then transferred to a glovebox and annealed at 130°C for 60 min. A 5 mg/mL solution of regioregular P3HT (4002-E, Rieke Metal Inc.) was prepared by dissolving it in dichlorobenzene (CB). The P3HT solution was stirred at 35°C for over 9 h in darkness. P3HT films were spin-coated onto the SiO_2/Si substrates at 1000 rpm for ∼40 s, and the films were annealed at 135°C for 30 min. 100 nm thick gold (Au) electrodes were then vapor-deposited onto each P3HT film at a pressure of less than 3×10^{-3} Pa using a shadow mask. The channels in the synaptic transistors were 25 μm long and 500 μm wide. UV glue was used to encapsulate each device.

2.2 Characterization

UV-visible (UV-vis) absorption spectra of the P3HT films were collected using a UV-vis-NIR spectrometer (Hitachi U4100). The surface morphologies and thicknesses of the P3HT film were characterized using an atomic force microscope (Veeco NanoScope V, Bruker). All of the devices were tested using a semiconductor parameter analyzer (FS480, PDA Co., Ltd) and a 532 nm laser as a light source. Optical stimulation was performed using an optical shutter equipped with a transistor-transistor logic (TTL) controller. An arbitrary waveform function generator (RIGOL DG5100) was used to modulate the optical shutter, and a PM 100D power meter (Thorlabs GmbH) was employed to measure the optical power density. The arbitrary waveform function generator was also used to directly deliver electrical pulses.

3 Results and discussion

In biological systems, synapses form the junctions between neuronal axons of presynaptic neurons, and the dendrites or cell bodies of postsynaptic neurons. A biological synapse is schematically illustrated in Figure 1(a). The transmission of information through a synapse begins with the stimulus-triggered release of neurotransmitters from synaptic vesicles in the presynaptic neuron into the synaptic cleft. The neurotransmitters are taken up by receptors in the postsynaptic neuron, which generates a postsynaptic current (PSC). An artificial Si/P3HT-based synapse, referred to here as a synaptic transistor, is shown in Figure 1(b). A presynaptic pulse was simulated by either delivering an optical pulse to the P3HT channel or delivering an electrical pulse to the Si back gate. Carriers in the P3HT channel acted as neurotransmitters, while the current collected at the drain (I_D) was the equivalent of the PSC.

A UV-vis absorption spectrum of P3HT is shown in Figure 1(c). P3HT absorbed visible light well, and it absorbed wavelengths in the range from 500 to 600 nm most strongly. We thus selected a 532 nm laser for optical stimulation of our synaptic transistors. The P3HT channel films were ∼33 nm thick and quite uniform with a surface roughness value of ∼0.49 nm (Figure 1(d)). Typical output curves of a synaptic transistor are shown in Figure 1(e). A shift in the back gate voltage V_G from 0 to −40 V I_D was

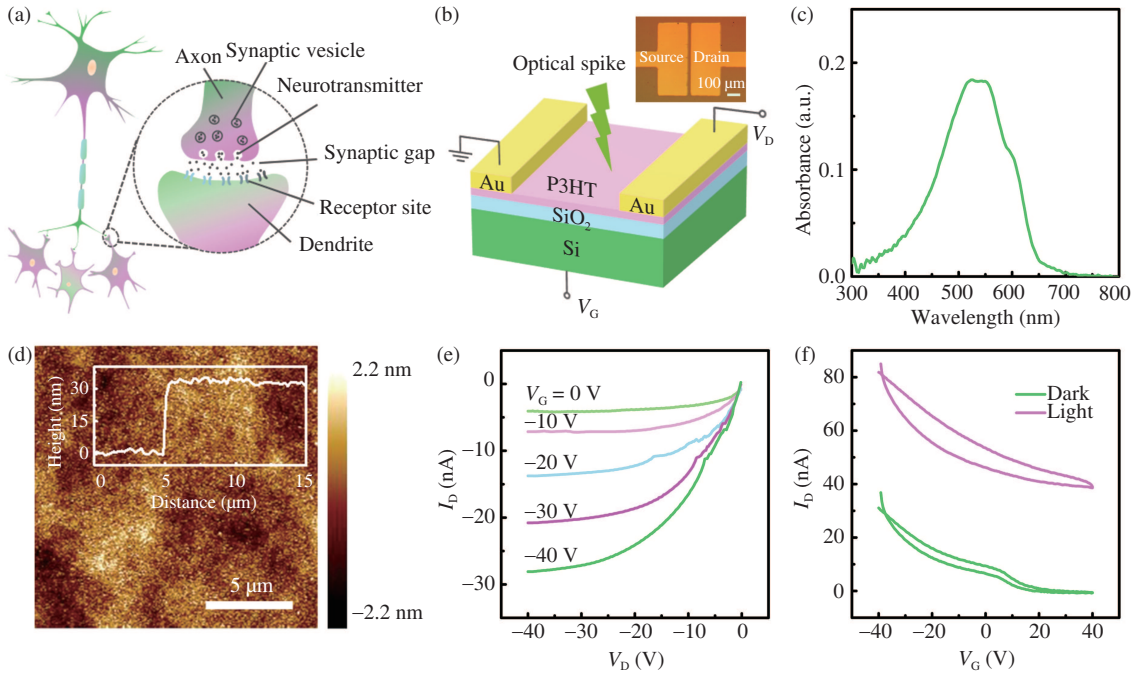

Figure 1 (Color online) Schematic illustrations of (a) a biological synapse and (b) an artificial Si/P3HT-based synaptic transistor. Inset: optical microscope image of the device. (c) UV-visible absorption spectrum of P3HT. (d) Atomic force microscope (AFM) images of a P3HT thin film. Inset: the thickness of the P3HT thin film measured via AFM line profiling. (e) Output curves of a typical synaptic transistor. (f) Transfer curves of the synaptic transistor obtained at V_D = 5 V in darkness and under optical illumination at (λ) 532 nm and a power density of 3.5 mW/cm^2.

consistent with the p-type conductivity of P3HT. The transfer curves of a synaptic transistor obtained at V_D = 5 V are shown in Figure 1(f). Hysteresis was observed when the voltage (V_G) was adjusted from −40 to 40 V, then back to −40 V. Hysteresis arose from the trapping and detrapping of carriers at the interface between P3HT and the SiO_2 gate oxide. This phenomenon is thoroughly documented in the literature on thin-film transistors based on organic semiconductors [36,37]. Hysteresis became more pronounced when P3HT was illuminated with the 532 nm laser (Figure 1(f)). This could be attributed to an excess of photogenerated carriers in P3HT, which could also be trapped and detrapped at the P3HT/SiO_2 interface.

The EPSC of a synaptic transistor induced by a single optical spike incident upon the P3HT channel is shown in Figure 2(a). The power density and duration of the optical pulse were 3.5 mW/cm^2 and 200 ms, respectively. The resting current (I_{D0}) of each synaptic transistor was set to zero, although the actual value was approximately 5.2 ± 0.8 nA. The EPSC reached a maximum of ∼16 pA, i.e., $EPSC_{max}$ = 16 pA, at the end of the optical pulse. After exposure to the optical pulse, the EPSC decayed with a relaxation time of ∼9.68 s. The relaxation time was the amount of time needed for the EPSC change from 90% to 10% of its original value [16,38]. The increase in the EPSC was related to an excess of photogenerated holes in P3HT, while EPSC decay was caused by the detrapping of excess photogenerated electrons that were trapped at the P3HT/SiO_2 interface. The magnitude of $EPSC_{max}$ depended on the duration of the optical pulse (Figure 2(b)). When the optical pulse duration was increased from 50 ms to 80 s, the $EPSC_{max}$ increased linearly, then gradually reached a plateau. This trend is also observed after the PSC of a biological synapse reaches its maximum value [39]. To analyze the working mechanism of the device, we chemically modified the surface of the SiO_2 layer by applying a (3-aminopropyl) trimethoxysilane (APTMS) self-assembled monolayer (SAM) [40]. The maximum EPSC was higher following surface modification, and it decayed more rapidly (Figure S3). This was because the SAM on SiO_2 effectively reduced the density of defects at the P3HT/SiO_2 interface [41]. We thus concluded that defects at the P3HT/SiO_2 interface played an essential role in the working mechanism of our synaptic devices.

Paired pulse facilitation is one of the most important phenomena affecting the short-term plasticity (STP) of a biological synapse. PPF could be simulated using our synaptic transistors. The EPSC induced by two consecutive optical pulses separated by a pulse interval of 300 ms is shown in Figure 2(c). The $EPSC_{max}$ induced by the second optical pulse (A_2) was clearly higher than that induced by the first pulse

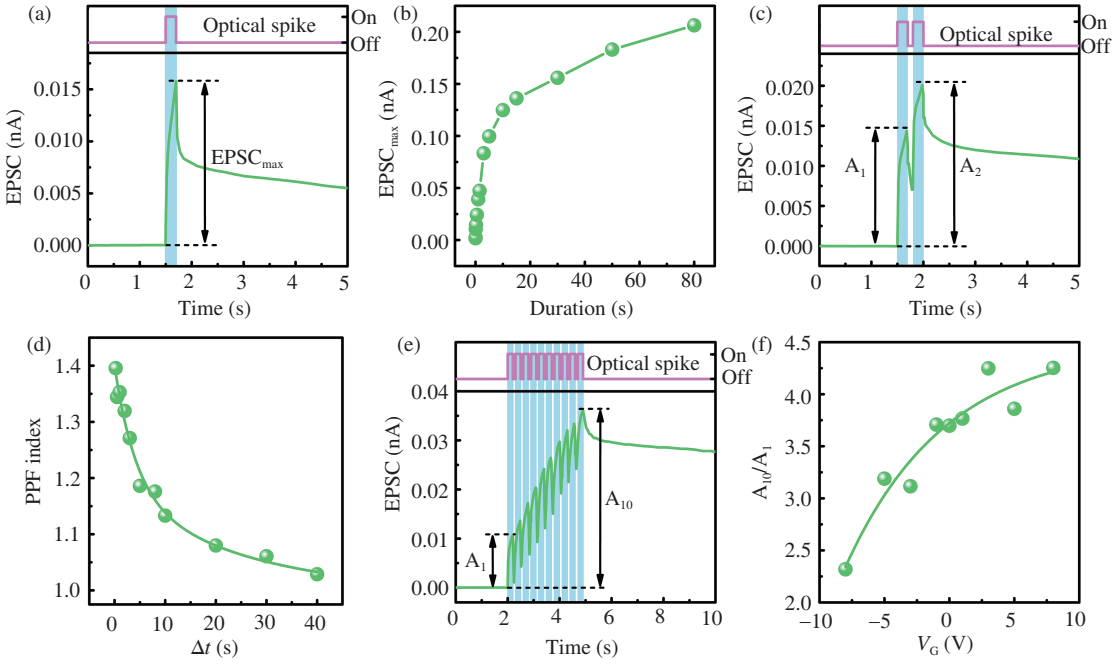

Figure 2 (Color online) (a) EPSC of a synaptic transistor induced by a single optical spike (λ = 532 nm) at V_D = 5 V and V_G = 0 V. The power density and duration of the optical pulse were 3.5 mW/cm^2 and 200 ms, respectively. (b) Dependence of the EPSC$_{max}$ on optical pulse duration. (c) EPSC induced by two consecutive optical pulses separated by a 300 ms pulse interval (Δt). (d) Dependence of the PPF index on Δt. (e) EPSC induced by 10 consecutive optical pulses. (f) Dependence of A$_{10}$/A$_1$ on V_G at V_D = 5 V.

(A$_1$). Upon completion of the second optical pulse, the EPSC decreased with a decay time of 35.61 s. The A$_2$/A$_1$ ratio is referred to as the PPF index. The dependence of the PPF index on the interval (Δt) between two consecutive optical spikes is illustrated in Figure 2(d). The PPF index increased to ~1.4, then decreased over time (Δt) until 300 ms had elapsed. We then fitted the data using a double exponential function. Rapid decay (τ_1) and slow decay (τ_2) of the PPF index were ~4.16 and 25.18 s, respectively. τ_2 was approximately one order of magnitude larger than τ_1, which was consistent with the dependence of the PPF index of a biological synapse on Δt [42].

Both the EPSC$_{max}$ and the EPSC decay time increased with the number of optical pulses (Figure S1). Figure 2(e) is a representative plot of the EPSC induced by ten consecutive optical pulses. The A$_{10}$/A$_1$ ratio of the EPSC$_{max}$ reached ~3.4 during the 10th optical pulse. The EPSC decay time following the 10th optical pulse was 54.48 s. These results were consistent with SNDP [43]. A similar transition could be induced by varying the optical pulse frequency from 0.13 to 4 Hz (Figure S2). Importantly, the Si back gate of the synaptic transistor could modulate synaptic plasticity (Figure 2(f)). When the back gate voltage was adjusted from −8 to 8 V, the A$_{10}$/A$_1$ ratio for ten consecutive optical pulses increased. As the back gate voltage changed, holes in P3HT were significantly depleted. Light-induced variations in the hole concentration in P3HT were consequently more pronounced. Biological neurons exist in an electrochemical environment. Global parameters, such as the concentrations of various hormones, regulate the overall neural network [44]. In this study, we applied a constant voltage to the Si back gates of several synaptic devices to mimic global regulation. We were clearly able to simulate biological homeostasis [45], which indicated that the Si substrates had an active functionality.

Our synaptic transistors could also be activated by electrical stimulation. Both an EPSC and an IPSC could be induced by applying positive and negative electrical spikes, respectively, at the Si back gate of a synaptic device (Figure 3(a)). Electrical stimulation was achieved by applying voltages of 0.1 V (positive) and −0.1 V (negative) for 200 ms. Whether the PSC was excitatory or inhibitory depended on the magnitude of the PSC immediately before the electrical pulse ended. The induction of the EPSC and IPSC by positive and negative electrical pulses was related to charging of the acceptor state and decharging of the donor state of the SiO_2 gate, respectively. This phenomenon was recently discussed in detail by Yin et al. [17]. Changes in the EPSC$_{max}$ and IPSC$_{max}$ depended on the duration of the electrical pulses (Figure 3(b)). The EPSC$_{max}$ initially increased, while the IPSC$_{max}$ initially decreased.

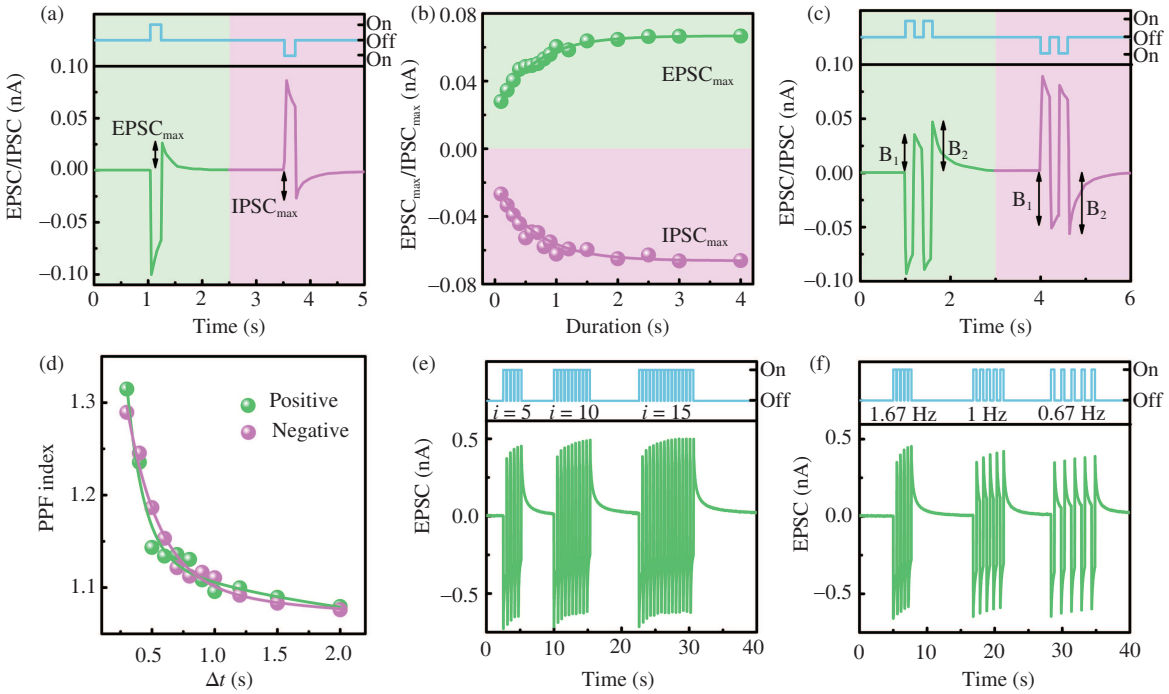

Figure 3 (Color online) (a) EPSC induced by a positive electrical spike (0.1 V) and IPSC induced by a negative electrical spike (−0.1 V) applied to the Si back gate of a synaptic transistor for 200 ms (V_D = 5 V). (b) Dependence of the EPSC$_{max}$ and IPSC$_{max}$ on electrical pulse duration. (c) PPFs of a synaptic transistor stimulated with two consecutive positive (0.1 V) or negative (−0.1 V) electrical pulses (Δt = 200 ms). (d) Dependence of the PPF index on the Δt of electrical stimulation. (e) EPSC induced by consecutive positive (0.1 V) electrical pulses with durations of 500 ms, where pulse quantity i = 5, 10, and 15. (f) EPSC induced by 10 positive (0.1 V) electrical pulses of 500 ms each at frequencies of 0.67, 1, and 1.67 Hz.

In both cases, saturation occurred when the duration of the electrical pulse was increased.

PPF in a synaptic transistor stimulated by two consecutive positive and two consecutive negative electrical pulses can be seen in Figure 3(c). The pulse duration and interval (Δt) were 200 and 300 ms, respectively. Like consecutive optical pulses, the second positive electrical pulse (B_2) induced a larger EPSC$_{max}$ than the first (B_1). IPSC induction by negative electrical stimulation followed the same trend. The dependence of the PPF index (B_2/B_1) on the Δt of electrical stimulation is illustrated in Figure 3(d). The PPF indices of the positive and negative electrical pulses decreased from ∼1.32 and 1.29 when Δt exceeded 300 ms. τ_1 and τ_2 associated with the decrease in the PPF index of positive electrical stimulation were 0.14 and 1.92 s, respectively. The τ_1 and τ_2 decay times associated with negative electrical stimulation were 0.26 and 2.23 s, respectively. The transitions resulting from both positive and negative electrical stimulation are examples of SRDP. The EPSCs induced by i (pulse quantity i = 5, 10, and 15) consecutive positive electrical spikes are shown in Figure 3(e). The maximum EPSC increased as i increased from 5 to 15, and the EPSC decayed more after electrical stimulation stopped. Similar changes were observed when the frequency of the positive electrical spikes increased from 0.67 to 1.67 Hz (Figure 3(f)).

Energy consumption by an optoelectronic device is one of its most important properties. Higher voltages usually lead to greater energy consumption. To minimize the amount of energy consumed by the synaptic devices, we used relatively low input voltages. The energy consumed by a synaptic device during a synaptic event can be calculated using

$$E = \int_0^t V \cdot I(t)\mathrm{d}t, \tag{1}$$

where $V(I)$ is the voltage (current) of the device, and t represents the duration of stimulation [18]. The energy required for stimulation is not included in this calculation. The minimum amount of energy consumed during both optical and electrical stimulation was ∼5.2 nJ, although less energy might have been consumed if we reduced the pulse duration and device dimensions.

It is well known that the information delivered to a biological nervous system by multiple sensory modalities must be processed in an integrated manner [46], which is made possible by the spatiotemporal

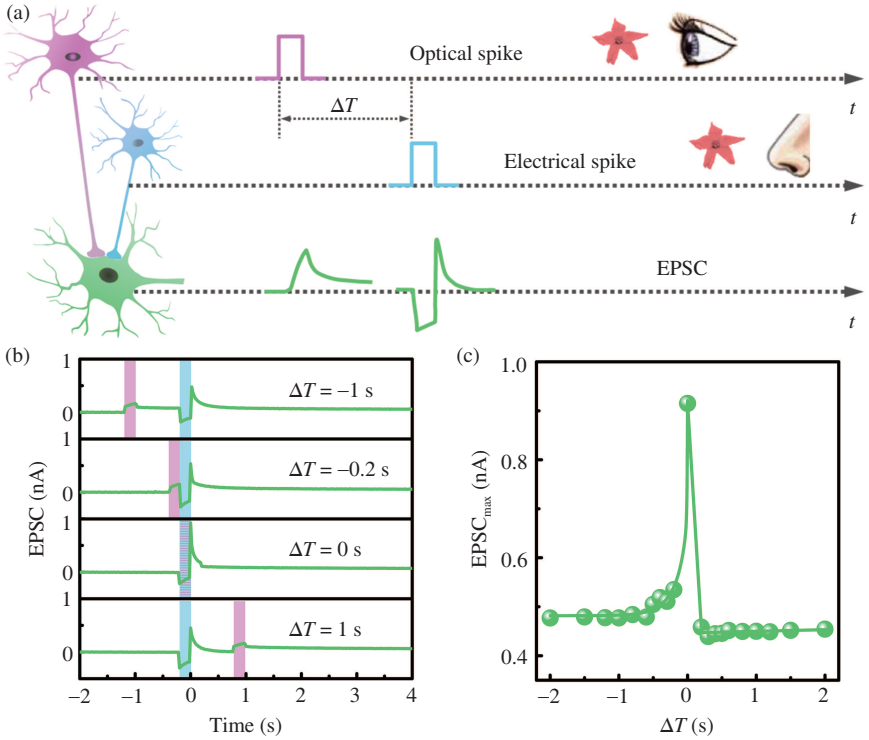

Figure 4 (Color online) (a) Schematic illustration of spatiotemporal synaptic integration. The optical and electrical pulses correspond to visual presynaptic neuron and olfactory presynaptic neuron stimulation, respectively. The power density and duration of the optical pulse are 1.5 W/cm^2 and 200 ms, respectively. The electrical pulse has a voltage of 0.5 V and a duration of 200 ms. (b) EPSC with intervals (ΔT) of -1 s, -0.2 s, 0 s, and 1 s between visual and olfactory stimulation. (c) Dependence of perception ($\mathrm{EPSC_{max}}$) on ΔT.

integration of synapses [47]. Our synaptic devices could spatiotemporally integrate optical and electrical stimuli, which enabled us to simulate cross-modal learning [48]. In Figure 4(a), the optical and positive electrical pulses correspond to visual presynaptic neuron and olfactory presynaptic neuron stimulation, respectively. The two pulses induced an EPSC in a postsynaptic multisensory integrative neuron [48]. How a flower is perceived depends on visual and/or olfactory stimulation, and perception may be evaluated by $\mathrm{EPSC_{max}}$.

The interval between visual and olfactory stimulation (ΔT) was varied to examine its effect on perception. The results obtained with ΔT values of -1, -0.2, 0, and 1 s are shown in Figure 4(b). ΔT was negative when the visual stimulus was delivered before the olfactory stimulus. ΔT equaled zero when the visual and olfactory stimuli were delivered simultaneously, and ΔT was positive when the visual stimulus was delivered after the olfactory stimulus. ΔT clearly affected the $\mathrm{EPSC_{max}}$, which indicated that timing had an important impact on synaptic integration [22,49,50]. The dependence of perception on the interval between visual and olfactory stimulation can be seen in Figure 4(c). The $\mathrm{EPSC_{max}}$ was highest when the visual and olfactory stimuli were delivered simultaneously, which meant that simultaneous stimulation resulted in maximum perception. When the visual stimulus preceded the olfactory stimulus, perception was more pronounced than it was with either visual or olfactory stimulation alone. When the visual stimulus was delivered after the olfactory stimulus, perception matched that triggered by an individual stimulus. This difference was attributed to much slower EPSC decay after the visual stimulus was delivered. The decay times for the visual and olfactory stimuli were 18.29 and 0.29 s, respectively. These results indicated that our Si/P3HT-based synaptic transistors could be employed to simulate cross-modal learning. It should be noted that the current V_{D} of 5 V used for our synaptic devices is somewhat high for Si-based integrated circuits. Additional experiments at lower V_{D} values are needed to ensure that the hybrid Si-based synaptic devices are fully compatible with Si-based optoelectronic integration.

4 Conclusion

We fabricated hybrid optoelectronic synaptic transistors based on P3HT and Si in this study. The de-

vices were stimulated by both optical and electrical pulses, and they mimicked several important synaptic functionalities. The Si/P3HT-based synaptic transistors demonstrated spatiotemporal integration during optical and electrical stimulation, which allowed us to simulate cross-modal learning. This study has important implications for the development of cost-effective Si-based optoelectronic synaptic devices with solution-processed organic semiconductors. We were inspired by recent progress in the application of Si and organic-inorganic perovskite hybrid structures in optoelectronic synaptic devices [51, 52]. We believe that hybrid devices comprised of Si and organic semiconductors are also promising for the development of novel Si-based optoelectronic synaptic devices, which should be useful for the construction of optoelectronic ANNs for neuromorphic computing.

Acknowledgements This work was mainly supported by National Key Research and Development Program of China (Grant Nos. 2017YFA0205704, 2018YFB2200101), Natural Science Foundation of China (Grant Nos. 91964107, 61774133), Fundamental Research Funds for the Central Universities (Grant No. 2018XZZX003-02), partial supported by Natural Science Foundation of China for Innovative Research Groups (Grant No. 61721005), and Zhejiang University Education Foundation Global Partnership Fund.

Supporting information Figures S1–S3. The supporting information is available online at info.scichina.com and link.springer.com. The supporting materials are published as submitted, without typesetting or editing. The responsibility for scientific accuracy and content remains entirely with the authors.

References

1 Merolla P A, Arthur J V, Alvarez-Icaza R, et al. A million spiking-neuron integrated circuit with a scalable communication network and interface. Science, 2014, 345: 668–673
2 Davies M, Srinivasa N, Lin T-H, et al. Loihi: a neuromorphic manycore processor with on-chip learning. IEEE Micro, 2018, 38: 82–99
3 Tang J, Yuan F, Shen X, et al. Bridging biological and artificial neural networks with emerging neuromorphic devices: fundamentals, progress, and challenges. Adv Mater, 2019, 31: 1902761
4 Zidan M A, Strachan J P, Lu W D. The future of electronics based on memristive systems. Nat Electron, 2018, 1: 22–29
5 Kuzum D, Yu S, Wong H-S P. Synaptic electronics: materials, devices and applications. Nanotechnology, 2013, 24: 382001
6 Upadhyay N K, Joshi S, Yang J J. Synaptic electronics and neuromorphic computing. Sci China Inf Sci, 2016, 59: 061404
7 Mao J Y, Zhou L, Zhu X, et al. Photonic memristor for future computing: a perspective. Adv Opt Mater, 2019, 7: 1900766
8 Yu F, Zhu L Q. Ionotronic neuromorphic devices for bionic neural network applications. Phys Status Solidi RRL, 2019, 13: pssr.201800674
9 Zhuge X, Wang J, Zhuge F. Photonic synapses for ultrahigh-speed neuromorphic computing. Phys Status Solidi (RRL), 2019, 13: 1900082
10 Dai S, Zhao Y, Wang Y, et al. Recent advances in transistor-based artificial synapses. Adv Funct Mater, 2019, 29: 1903700
11 Atabaki A H, Moazeni S, Pavanello F, et al. Integrating photonics with silicon nanoelectronics for the next generation of systems on a chip. Nature, 2018, 556: 349–354
12 Thomson D, Zilkie A, Bowers J E, et al. Roadmap on silicon photonics. J Opt, 2016, 18: 073003
13 Rosenbluth D, Kravtsov K, Fok M P, et al. A high performance photonic pulse processing device. Opt Express, 2009, 17: 22767–22772
14 Tan H, Ni Z, Peng W, et al. Broadband optoelectronic synaptic devices based on silicon nanocrystals for neuromorphic computing. Nano Energy, 2018, 52: 422–430
15 Ni Z, Wang Y, Liu L, et al. Hybrid structure of silicon nanocrystals and 2D WSe2 for broadband optoelectronic synaptic devices. In: Proceedings of 2018 IEEE International Electron Devices Meeting (IEDM), San Francisco, 2018. 1–4
16 Zhao S, Ni Z, Tan H, et al. Electroluminescent synaptic devices with logic functions. Nano Energy, 2018, 54: 383–389
17 Yin L, Han C, Zhang Q, et al. Synaptic silicon-nanocrystal phototransistors for neuromorphic computing. Nano Energy, 2019, 63: 103859
18 Li Y Y, Wang Y, Yang D R, et al. Recent progress on optoelectronic synaptic devices (in Chinese). Sci Sin Inform, 2020, 50: 118–138
19 Chen B, Yu Z, Liu K, et al. Grain engineering for perovskite/silicon monolithic tandem solar cells with efficiency of 25.4%. Joule, 2019, 3: 177–190
20 Ni Z, Ma L, Du S, et al. Plasmonic silicon quantum dots enabled high-sensitivity ultrabroadband photodetection of graphene-based hybrid phototransistors. ACS Nano, 2017, 11: 9854–9862
21 Chen S, Li W, Wu J, et al. Electrically pumped continuous-wave III-V quantum dot lasers on silicon. Nat Photon, 2016, 10: 307–311
22 Qin S, Wang F, Liu Y, et al. A light-stimulated synaptic device based on graphene hybrid phototransistor. 2D Mater, 2017, 4: 035022
23 Wang Y, Lv Z, Chen J, et al. Photonic synapses based on inorganic perovskite quantum dots for neuromorphic computing. Adv Mater, 2018, 30: 1802883
24 Wang S, Chen C, Yu Z, et al. A MoS2/PTCDA hybrid heterojunction synapse with efficient photoelectric dual modulation and versatility. Adv Mater, 2019, 31: 1806227
25 Wang K, Dai S, Zhao Y, et al. Light-stimulated synaptic transistors fabricated by a facile solution process based on inorganic perovskite quantum dots and organic semiconductors. Small, 2019, 15: 1900010
26 Wang R, Wang Y, Wu C, et al. Direct observation of conductive polymer induced inversion layer in n-si and correlation to solar cell performance. Adv Funct Mater, 2020, 30: 1903440
27 Mao J Y, Hu L, Zhang S-R, et al. Artificial synapses emulated through a light mediated organic-inorganic hybrid transistor. J Mater Chem C, 2019, 7: 48–59
28 Fang L, Dai S, Zhao Y, et al. Light-stimulated artificial synapses based on 2D organic field-effect transistors. Adv Electron Mater, 2020, 6: 1901217
29 Wu X, Chu Y, Liu R, et al. Pursuing polymer dielectric interfacial effect in organic transistors for photosensing performance optimization. Adv Sci, 2017, 4: 1700442

30 Dai S, Wu X, Liu D, et al. Light-stimulated synaptic devices utilizing interfacial effect of organic field-effect transistors. ACS Appl Mater Interf, 2018, 10: 21472–21480
31 Arias A C, MacKenzie J D, McCulloch I, et al. Materials and applications for large area electronics: solution-based approaches. Chem Rev, 2010, 110: 3–24
32 Berger P R, Kim M. Polymer solar cells: P3HT:PCBM and beyond. J Renew Sustain Energy, 2018, 10: 013508
33 Zhao S, Pi X, Mercier C, et al. Silicon-nanocrystal-incorporated ternary hybrid solar cells. Nano Energy, 2016, 26: 305–312
34 Shalu C, Yadav N, Bhargava K, et al. All organic near ultraviolet photodetectors based on bulk hetero-junction of P3HT and DH6T. Semicond Sci Technol, 2018, 33: 095021
35 Zhao S, Wang Y, Huang W, et al. Developing near-infrared quantum-dot light-emitting diodes to mimic synaptic plasticity. Sci China Mater, 2019, 62: 1470–1478
36 Chu Y, Wu X, Lu J, et al. Photosensitive and flexible organic field-effect transistors based on interface trapping effect and their application in 2D imaging array. Adv Sci, 2016, 3: 1500435
37 Yogev S, Matsubara R, Nakamura M, et al. Fermi level pinning by gap states in organic semiconductors. Phys Rev Lett, 2013, 110: 036803
38 Saidaminov M I, Adinolfi V, Comin R, et al. Planar-integrated single-crystalline perovskite photodetectors. Nat Commun, 2015, 6: 8724
39 Yang Y, Lisberger S G. Purkinje-cell plasticity and cerebellar motor learning are graded by complex-spike duration. Nature, 2014, 510: 529–532
40 Alibart F, Pleutin S, Guérin D, et al. An organic nanoparticle transistor behaving as a biological spiking synapse. Adv Funct Mater, 2010, 20: 330–337
41 Horii Y, Ikawa M, Sakaguchi K, et al. Investigation of self-assembled monolayer treatment on SiO2 gate insulator of poly(3-hexylthiophene) thin-film transistors. Thin Solid Films, 2009, 518: 642–646
42 Zucker R S, Regehr W G. Short-term synaptic plasticity. Annu Rev Physiol, 2002, 64: 355–405
43 Jackman S L, Regehr W G. The mechanisms and functions of synaptic facilitation. Neuron, 2017, 94: 447–464
44 Gkoupidenis P, Koutsouras D A, Malliaras G G. Neuromorphic device architectures with global connectivity through electrolyte gating. Nat Commun, 2017, 8: 15448
45 Lerch M M, Grinthal A, Aizenberg J. Viewpoint: homeostasis as inspiration-toward interactive materials. Adv Mater, 2020, 32: 1905554
46 Srinivasan M V, Zhang S W, Zhu H. Honeybees link sights to smells. Nature, 1998, 396: 637–638
47 Steward O. Functional neuroscience. Trends Neurosci, 2000, 23: 12
48 Guo J, Guo A. Crossmodal interactions between olfactory and visual learning in drosophila. Science, 2005, 309: 307–310
49 Alquraishi W, Fu Y, Qiu W, et al. Hybrid optoelectronic synaptic functionality realized with ion gel-modulated In_2O_3 phototransistors. Org Electron, 2019, 71: 72–78
50 Jiang J, Hu W, Xie D, et al. 2D electric-double-layer phototransistor for photoelectronic and spatiotemporal hybrid neuromorphic integration. Nanoscale, 2019, 11: 1360–1369
51 Yin L, Huang W, Xiao R, et al. Optically stimulated synaptic devices based on the hybrid structure of silicon nanomembrane and perovskite. Nano Lett, 2020, 20: 3378–3387
52 Huang W, Hang P J, Wang Y, et al. Zero-power optoelectronic synaptic devices. Nano Energy, 2020, 73: 104790